American Mineralogist, Volume 59, pages 587–597, 1974

The Generation of N_2–CO_2–H_2O Fluids for Use in Hydrothermal Experimentation I. Experimental Method and Equilibrium Calculations in the C–O–H–N System

JOHN R. HOLLOWAY

Division of Geochemistry, Department of Chemistry, Arizona State University, Tempe, Arizona 85281

ROBERT L. REESE

Department of Geology, Arizona State University, Tempe, Arizona 85281

Abstract

The activities of H_2O and CO_2 can be varied independently in hydrothermal experiments by using certain C–O–H–N compounds to generate an essentially ternary H_2O–CO_2–N_2 fluid. For an initial bulk composition, the species composition of the fluid is a function of pressure, temperature, and hydrogen fugacity. The results of equilibrium calculations in the system C–O–H–N illustrate these relationships for typical experimental hydrogen fugacities in the range to 10 kbar and 800 to 1200°C. Unless the hydrogen fugacity is externally controlled at low levels, the actual mole fraction of H_2O in the fluid may differ considerably from the nominal mole fraction in the ternary system, particularly when the mole fraction of H_2O is low. The formation of graphite, nitrides, and oxynitrides, and changes in fluid composition due to reaction with condensed species, are experimental problems which can be avoided or minimized.

Introduction

In nature the fluid phases involved in many geologically important equilibria are usually impure with H_2O and CO_2 as major species. Early experimental studies usually duplicated only the limiting situation in which the fluid phase consisted of just one volatile species, and the equilibrium pressure of that species was equal to total pressure. Several investigators have therefore devised methods of controlling P_{H_2O} and P_{CO_2} at values less than P_T by use of (1) mixtures of H_2O and H_2 (Shaw, 1967), (2) complex C–H–O fluids (Eugster and Skippen, 1967), (3) mixtures of H_2O and CO_2 in which the fluid controls the H_2O/CO_2 ratio (Holloway, Burnham, and Millhollen, 1968), and (4) mixtures of H_2O and CO_2 in which the fluid is analyzed at the end of the run (Greenwood, 1967; Metz, 1967). However, each of the above methods has disadvantages which limit its usefulness. For instance, the use of methods (1) and (2) results in fixed values of oxygen fugacity (f_{O_2}) which may not be in the desired range; if relatively low values of P_{H_2O} are achieved using method (3), there is the possibility of crystallizing unwanted carbonates; and method (4) requires analysis of the fluid at the termination of each run.

This paper describes a method for generating H_2O–CO_2–N_2 fluids during experiments, thus allowing the independent variation of P_{H_2O}, P_{CO_2}, and f_{O_2} at geologically significant temperatures and pressures. Important practical aspects of this method, namely the effects of P, T, and f_{H_2} on fluid compositions, are evaluated by means of equilibrium calculations. An experimental application of the method is presented in part II of this study (Kesson and Holloway, 1974).

Experimental Method

A fluid phase containing the desired proportions of H_2O, CO_2, and N_2 is produced by the thermal decomposition of one or more C–O–H or C–O–H–N solid compounds sealed inside an inert metal capsule along with the sample. This is an extension of the method described by Holloway *et al* (1968) and Holloway (1973) for generating H_2O–CO_2 fluids from mixtures of oxalic acid dihydrate + H_2O or from oxalic acid dihydrate + anhydrous oxalic acid.

Several compounds which can be used either

TABLE 1. Symbols and Abbreviations Used

P_i	Equilibrium partial pressure of species i
P_t	Total pressure
f_i	Fugacity of species i
X_i	Actual mole fraction of species i
$X(\text{nom})_i$	Mole fraction of CO_2, N_2 or H_2O in a fluid assuming complete loss of 'excess' H_2.
δ_{H_2O}	$X_{H_2O} - X(\text{nom})_{H_2O}$
HM, OH	Hematite + Magnetite + O-H fluid.
MH, OH	Manganosite ($Mn_{1-x}O$) + Hausmannite (Mn_3O_4) + O–H fluid.
NNO, OH	NiO + Ni + O–H fluid
QFM, OH	Quartz + fayalite (Fe_2SiO_4) + Magnetite + O–H fluid
WM, OH	Wustite ($Fe_{1-x}O$) + Magnetite + O–H Fluid.

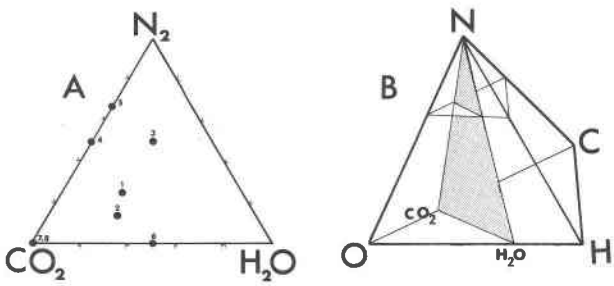

FIG. 1. (A) Nominal compositions of fluids 1–8 listed in Table 2. Expressed in mole fractions. (B) Schematic representation of the C–O–H–N system. The CO_2–H_2O–N plane is stippled; the unstippled plane near the N apex is at the ratio $N/(C + O + H) = 3/2$.

singly or in combination to generate ternary fluids in the system C–O–H–N are listed in Table 2 with their melting or decomposition points at 1 bar and their nominal species composition at P and T (mole fractions of H_2O, CO_2, N_2 and O_2). The nominal species compositions are shown in Figure 1A. The decomposition of compounds 1 to 7 produces excess H_2; the nominal mole fractions listed in Table 2 assume *complete* loss of this excess H_2. The excess H_2- producing compounds are designated as such because the initial fluid produced by their decomposition contains free H_2 when oxygen is allocated to C as CO_2 and to H as H_2O. Prior to the loss of excess H_2, the fluids lie in the H_2O–CO_2–N–H volume of the C–O–H–N tetrahedron illustrated in Figure 1B, and the mole fractions of H_2O, CO_2, N_2, and H_2 in the initial fluids are also given in Table 2. Compounds 9 to 15 decompose to produce excess oxygen, and can be conveniently used in combination with excess H_2-producing compounds to limit the amount of H_2 produced, and thus avoid certain experimental problems noted later in this paper. Silver, palladium, and platinum compounds decompose during experiments to precipitate the metal.

Most of the compounds are subject to large variations in water content if exposed to the atmosphere for a period of time. However, their stoichiometric compositions can be maintained if they are stored

TABLE 2. Fluid Generating Compounds

Key to Fig. 1	Compound name	Empirical Formula	One atm. Melting or decomposition point (°C)	Initial mole fraction of: N_2	CO_2	H_2O	H_2	O_2	Nominal mole fraction of: N_2	CO_2	H_2O	O_2
1	Ammonium oxalate	$C_2H_8O_4N_2 \cdot H_2O$	100	.125	.25	.125	.50		.25	.50	.25	
2	Ammonium oxalate, acid	$C_2H_5O_4 \cdot H_2O$	170	.083	.333	.167	.417		.14	.57	.29	
3	Guanidine nitrate	$CH_5N_3 \cdot HNO_3$	214	.333	.167	.167	.333		.50	.25	.25	
4	Guanidine carbonate**	$C_2H_{10}N_6 \cdot H_2CO_3$	197	.20	.20		.60		.50	.50		
5	Nitro-guanidine	$CH_4O_2N_4$	232	.40	.20		.40		.67	.33		
6	Oxalic acid, dihydrate	$H_2C_2O_4 \cdot 2H_2O$	101		.40	.40	.20			.50	.50	
7	Oxalic acid, anhydrous	$H_2C_2O_4$	190		.667		.333			1.00		
8	Silver oxalate	AgC_2O_4	140		1.00					1.00		
9	Ammonium nitrate	NH_4NO_3	170	.286		.571		.143	.29		.57	.14
10	Silver nitrate	$AgNO_3$	212	.25				.75	.25			.75
11	Silver nitrite	$AgNO_2$	140	.333				.667	.33			.67
12	Silver carbonate	Ag_2CO_3	218		.667			.333	.67			.33
13	Silver oxide	Ag_2O	300					1.00				1.00
14	Platinum dioxide	PtO_2	450					1.00				1.00
15	Palladium monoxide	PdO	870					1.00				1.00

*Mole fractions calculated assuming oxygen combines with carbon to form CO_2, with hydrogen to form H_2O and remaining H_2 is removed from the system.

**Mole fractions calculated assuming the addition of 3 moles of H_2O for each mole of guanidine carbonate.

in well-sealed containers. It must be noted that most of the compounds can react explosively if exposed to air at moderate temperatures, and consequently great care is needed during capsule welding. The sample capsule can be kept sufficiently cool during welding by immersing its lower portion in ice + water, dry ice + alcohol, or liquid nitrogen. Excellent technical advice on the preparation of sample capsules is given by Huebener (1971).

Equilibrium Calculations

Introduction

The equilibrium calculations discussed in this section have allowed us to predict the variations in fluid compositions as H_2 diffuses through the sample capsule walls during the initial stages of an experiment, and also to specify the equilibrium species compositions when f_{H_2} is externally controlled.

Equilibrium species compositions have been calculated for selected bulk compositions throughout the C–H–O system with closely spaced composition points chosen near the H_2O–CO_2 join. Similar calculations have been made in the C–O–H–N system at selected ratios of N/(C + H + O) for several of the fluids produced by compounds listed in Table 2. The calculations were made at 1, 5, and 10 kbar and 800, 1000, and 1200°C plus 500°C at 1 kbar.

Equilibria involving graphite + fluid in the C–H–O system have been calculated for a wide range of *P-T* conditions by French and Eugster (1965) and French (1966). Calculations in the C–O–H–N system have been made by Dayhoff *et al* (1967) and have provided useful guidelines for our studies. However, most of the equilibria presented in this paper cover *P*, *T*, and bulk composition conditions which have not been covered in those investigations.

Method

The equilibrium calculations involve minimizing the Gibbs free energy of the system under consideration, using a technique known as the "NASA method" (Huff, Gordon, and Morrell, 1951) as described by van Zeggern and Storey, (1970). The computation utilizes a modified version of a program written by Gordon and McBride (1971); the modifications are discussed in detail by Reese (1973). Important modifications include the consideration of the fugacity coefficients of fluid species, and the consideration of molar volumes for solid phases. Thermodynamic data were taken from Robie and Waldbaum (1968) and Stull and Prophet (1971). The following species were considered in the calculations: graphite, CH, CH_2O, CO, CO_2, C_2H, C_2H_4, C, C_2, C_3, C_4, C_5, H, HO_2, H_2O, O, O_2, CH_2, CH_3, CH_4, C_2H_2, C_2O, C_3O_2, HCO, H_2, H_2O_2, OH, CN_2, C_2N, HCN, HNCO, N, NH, NH_2, NH_3, NO_2, N_2H_4, N_2O_4, CN, CN_2, C_2N_2, HNO, NCO, NO, N_2O, N_2, and N_3.

Accuracy

The numerical programming technique used is essentially error-free for problems of this type. Consequently the accuracy of the calculations depends on (1) the Gibbs free energy data at one atmosphere, (2) the fugacity coefficients at *P* and *T*, (3) the molar volume of graphite (the only crystalline phase), and (4) the absence of any species not explicitly considered. Inclusion of 47 species in the calculations, including all species detected by qualitative gas chromatographic analyses of C–O–H–N fluids produced in experimental runs, makes an error of type (4) unlikely. The one atmosphere free energy data are accurately known for gaseous species. The molar volume of graphite is accurately known and is assumed to be independent of *P* and *T* in the calculations. Because thermal expansion and compressibility are small and tend to cancel, this assumption should not introduce significant error. The largest source of uncertainty is undoubtedly the species fugacity coefficients, first in the values for the pure species, and second in the effects of fluid composition.

The fugacity coefficients of the pure species are known with varying degrees of uncertainty. The coefficients for H_2O are computed (Holloway, Eggler, and Davis, 1971) from precise and accurate *P-V-T* data (Burnham, Holloway, and Davis, 1969), and the error in these coefficients has a negligible effect on the final results of the equilibrium calculations. Fugacity coefficients for H_2 are calculated using equations given by Shaw and Wones (1964) and agree within 2 percent with coefficients derived from experimental *P-V-T* data (Presnall, 1969). The fugacity coefficients for CO, CO_2, CH_4, HCN, N_2, NH_3, N_2H_4, N_2O, NO, N_2O_4, and O_2 were computed from the Redlich-Kwong corresponding state equation (Redlich and Kwong, 1949) using a numerical technique proposed by Edmister (1968).[1] Values for

[1] A brief description of the calculations and a FORTRAN IV subroutine are contained in Appendix I. Appendices I and II can be obtained by ordering NAPS Document 02344 from ASIS c/o Microfiche Publications, 305 East 46th Street, New York, N. Y. 10017. Please remit in advance $1.50 for microfiche or $25.25 for photocopy. Please check the most recent issue of this journal for the current address and prices.

the critical temperatures and pressures required by the Redlich-Kwong equation were taken from Matthews (1972). The fugacity coefficients for all other species were set equal to unity.

For lack of other data, all fluid species are here assumed to mix ideally following the Lewis and Randall rule (Lewis and Randall, 1961). French (1966) has discussed the probable error involved in that assumption and concludes that calculated compositions are in error by no more than a factor of two for minor species.

The accuracy of the Redlich-Kwong fugacity coefficients can be evaluated by comparison with coefficients derived from experimental data. The Redlich-Kwong fugacity coefficients for CO_2 agree within 5 percent with values derived from the free energy data of Sharp (1962). Sharp's values were obtained from *P-V-T* data to pressures of 1.4 kbar (Kennedy, 1954). The Redlich-Kwong fugacity coefficients for H_2O lie within 20 percent of the coefficients computed from *P-V-T* data for the entire *P-T* range of this study. Because corresponding state methods are less accurate for H_2O than for the other species considered (Lewis and Randall, 1961), it is reasonable to assume a maximum relative error of ± 10 percent in the Redlich-Kwong fugacity coefficients.

Errors of this magnitude will affect the results of the equilibrium calculations, and the final uncertainty will depend on the particular equilibria involved. For example, variations of ± 10 percent in the fugacity coefficients for H_2 and CH_4 can result in a maximum uncertainty of ± 100°C in the equilibrium temperature for the appearance of graphite in the reaction $C + 2H_2 = CH_4$. In the present study, the calculated values of most interest are the mole fractions of H_2O, CO_2, and N_2 for a given value of X_{H_2}. Uncertainties in those values were evaluated by fixing *P*, *T*, and bulk composition and systematically varying the fugacity coefficients of the major species by ± 20 percent. The results of that test indicate maximum errors of ± 0.002 in the mole fractions of H_2O, CO_2, N_2, and H_2, and errors of ± 0.1 in $\log_{10} f_{O_2}$. Errors of that magnitude should have no effect on the conclusions reached in this paper.

Results of Equilibrium Calculations

The results of equilibrium calculations for the system C–H–O and the system C–O–H–N are presented primarily in graphical form, together with one representative table (Table 3). More extensive tables are contained in Appendix II (see footnote 1).

I. The System C–H–O

Introduction

Dayhoff *et al* (1967) divided the C–H–O system into the following regions (Fig. 2): (1) H_2O–CO_2–O; O_2 is always a major species along with H_2O and CO_2, and all other species are present in extremely low concentrations. For example, for bulk compositions lying exactly on the H_2O–CO_2 join, X_{H_2} is $<10^{-7}$ and decreases rapidly as bulk compositions approach O. (2) H_2O–CH_4–H; major species are CH_4, H_2 and H_2O, and the common minor species are CO, CO_2 and

TABLE 3. Calculated Compositions of Guanidine Nitrate Fluids as a Function of X_{H_2} at 800° and One Kbar

	(1)	(2)	(3)	(4)	(5)	(6)	(7)	(8)
Bulk Composition*								
H_2	.333	.2727	.2000	.1111	.0431	.0196	.0099	.0000
H_2O	.1667	.1818	.2000	.2222	.2392	.2353	.2475	.2500
N_2	.3333	.3636	.4000	.4444	.4785	.4706	.4950	.5000
CO_2	.1667	.1818	.2000	.2222	.2392	.2353	.2475	.2500
Major Species**								
H_2†	.0522	.0444	.0362	.0263	.0157	.0087	.0046	(7.608)
H_2O	.3659	.3420	.3146	.2834	.2618	.2552	.2527	.2500
N_2	.3847	.4065	.4308	.4589	.4811	.4905	.4951	.5000
CO_2	.0988	.1255	.1562	.1926	.2225	.2357	.2425	.2500
CO	.0164	.0190	.0210	.0208	.0155	.0093	.0051	.0000
CH_4	.0781	.0595	.0388	.0164	.0028	.0003	.0000	(25.672)
NH_3	.0039	.0031	.0024	.0015	.0007	.0003	.0001	(11.840)
Minor Species***								
CH	25.394	25.407	25.460	25.626	26.062	26.655	27.344	---‡
CH_2	18.061	18.109	18.207	18.422	18.989	19.710	20.529	---
CH_3	8.416	8.499	8.640	8.945	9.603	10.452	11.412	---
C_2H	19.002	18.992	19.054	19.317	20.070	21.128	22.347	---
C_2H_2	9.766	9.792	9.898	10.231	11.095	12.281	13.639	---
C_2H_4	5.994	6.089	6.284	6.755	7.844	9.286	10.924	---
CH_2O	5.788	5.795	5.840	5.982	9.603	6.812	7.355	17.869
CN	17.763	17.729	17.725	17.808	18.120	18.580	19.117	---
CNN	27.113	27.066	27.050	27.119	27.421	27.876	.000	---
CN_2	21.914	21.868	21.852	21.921	22.222	22.679	23.214	---
C_2N	22.514	22.458	22.463	22.643	23.273	24.199	25.275	---
C_2N_2	13.631	13.563	13.556	13.722	14.340	15.262	16.336	---
C_2O	19.565	19.479	19.445	19.545	19.995	20.679	21.482	---
C_2O_2	13.151	13.002	12.925	13.028	13.604	14.509	5.575	---
H	9.957	9.993	10.037	10.106	10.221	10.349	10.489	13.121
HCO	10.443	10.415	10.416	10.488	10.731	11.079	11.482	19.363
HCN	5.907	5.908	5.949	6.101	6.522	7.111	7.788	20.928
HNO	16.502	16.485	16.464	16.426	16.340	16.219	16.081	13.451
HCNO	6.309	6.269	6.257	6.315	6.546	6.890	7.292	15.170
HO_2	22.502	22.456	22.396	22.278	22.012	21.650	21.239	13.349
H_2O_2	17.181	17.169	17.153	17.105	16.951	16.717	16.445	11.189
N	21.483	21.471	21.458	21.445	21.438	21.433	21.431	21.429
NCO	16.613	16.538	16.483	16.472	16.592	16.807	17.069	22.314
NH	16.202	16.225	16.257	16.313	16.418	16.541	16.679	19.310
NH_2	9.925	9.983	10.059	10.184	10.401	10.653	10.931	16.194
NO	13.871	13.818	13.753	13.646	13.520	13.271	12.993	7.730
NO_2	23.496	23.402	23.286	23.085	22.696	22.201	21.648	11.124
N_2H_4	13.114	13.230	13.382	13.632	13.944	14.448	15.004	25.531
N_2O	16.655	16.590	16.513	16.392	16.255	16.001	15.722	10.456
N_3	22.223	22.187	22.150	22.108	22.080	22.068	22.062	22.055
O	20.387	20.346	20.294	20.200	20.013	19.768	19.492	14.231
OH	11.705	11.699	11.691	11.667	11.590	11.473	11.338	8.709
O_2	20.046	19.964	19.860	19.673	19.294	18.804	18.253	7.730
$-\log_{10}(f_{O_2})$	17.14	17.06	16.95	16.77	16.093	15.603	15.052	4.529

*Expressed as mole fraction with all of H, N, C and O assigned to the four species listed. Guanidine nitrate has the bulk composition given in column 1.

**Expressed as actual mole fraction at equilibrium.

***Expressed as $-\log_{10}$(mole fraction).

†The corresponding X_{H_2} values for buffers are: Wm,OH = 0.1169, QFM,OH = 0.0122, and NNO,OH = 0.0047.

‡Blanks indicate the value was less than 10^{-28}.

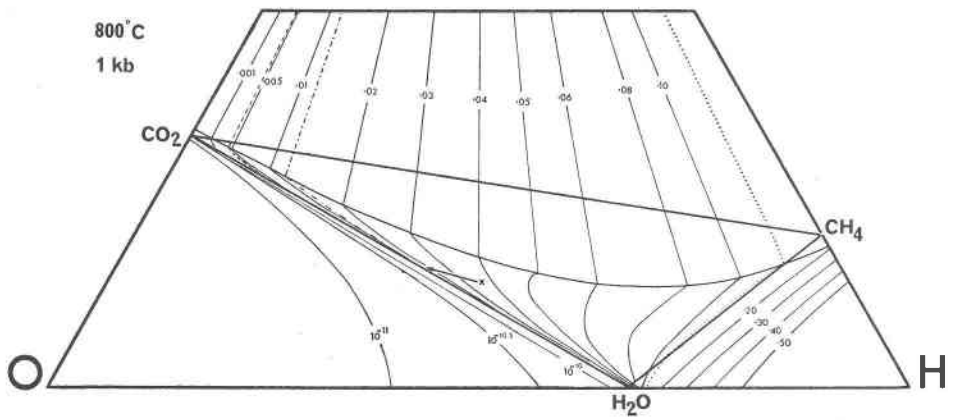

FIG. 2. Contours in the C–H–O system. The C apex (not shown) lies at the top apex of the equilateral triangle. Numbers on contours represent X_{H_2}. The curved line falling close to the CO_2 and CH_4 compositions is the graphite boundary, graphite being stable in the region above the line. Hydrogen buffer contours are shown by the dashed line for NNO, OH; the dot-dashed line for QFM, OH; and the dotted line for WM, OH. The point indicated by 'X' indicates the initial composition of a fluid generated from oxalic acid dihydrate.

C_2H_4. (3) H_2O–CO_2–CH_4; this is the region of prime interest in the present study. Most of the graphite boundary is contained within this triangle. (4) The graphite stability field; the species composition of the fluid at a fixed P and T is fixed by the O/H ratio of the bulk composition. Equilibria in this region have been extensively discussed by French and Eugster (1965) and French (1966).

Qualitative differences between the four regions are illustrated by X_{H_2} contours in Figure 2. In this paper we are concerned with compositions near the CO_2–H_2O join in which f_{H_2} is either controlled externally or is floating at the ambient level of the pressure vessel. In either case the X_{H_2} values[2] are usually between MH, OH, and QFM, OH (see Whitney, 1972). It can be seen in Figure 2 that the region of interest is thus restricted to a narrow strip parallel to and including the H_2O–CO_2 join. In order to illustrate compositional variations in this region, diagrams have been constructed by expanding the narrow strip in the direction perpendicular to the H_2O–CO_2 join. One such diagram is shown in Figure 3, where the vertical axis represents C + H in excess of H_2O + CO_2. Note particularly the directions of the C and H apices of the C–H–O equilateral triangle on the rectangular diagram. Directional lines ("to H" and "to C") show the path that bulk compositions would follow due to addition or subtraction of H at a constant C/O ratio, or of C at a constant H/O ratio. They are *hydrogen reaction lines* and *carbon reaction lines* respectively and are exactly analogous to the oxygen reaction lines discussed by Muan and Osborn (1965). Note that because of the nature of the scale expansion, the angle between the reaction lines and the coordinate axes changes across the diagram. X_{H_2O} contours are shown and plot as straight lines on this diagram. Also shown are the contours which correspond to the X_{H_2} produced by the MH, NNO, and QFM oxygen buffers plus an O–H fluid. These contours are henceforth referred to as *hydrogen buffer lines*.

The Effect of f_{H_2} on Fluid Composition

The relationships between fluid compositions and externally controlled f_{H_2} have been investigated at a representative P and T (1 kbar, 800°C) and are contained in Figure 3. These relationships are relevant to several experimental methods commonly used to generate CO_2 + H_2O fluids. For example, decomposition of oxalic acid dihydrate produces a fluid whose bulk composition lies at **X** in Figure 3. The intermediate products of the decomposition process are unknown, but qualitative gas chromatographic analyses indicate that after only a few minutes at temperatures above 500°C the major species are CO_2, H_2O, and H_2. If the initial fluid at **X** is contained in a capsule permeable to H_2 and if X_{H_2} is externally controlled by QFM, OH, then H_2 will diffuse out of

[2] The quantity X_{H_2} is used in preference to f_{H_2} because it is relatively insensitive to P and T whereas the value of f_{H_2} varies over a wide range. X_{H_2} is thus a more convenient numeric quantity.

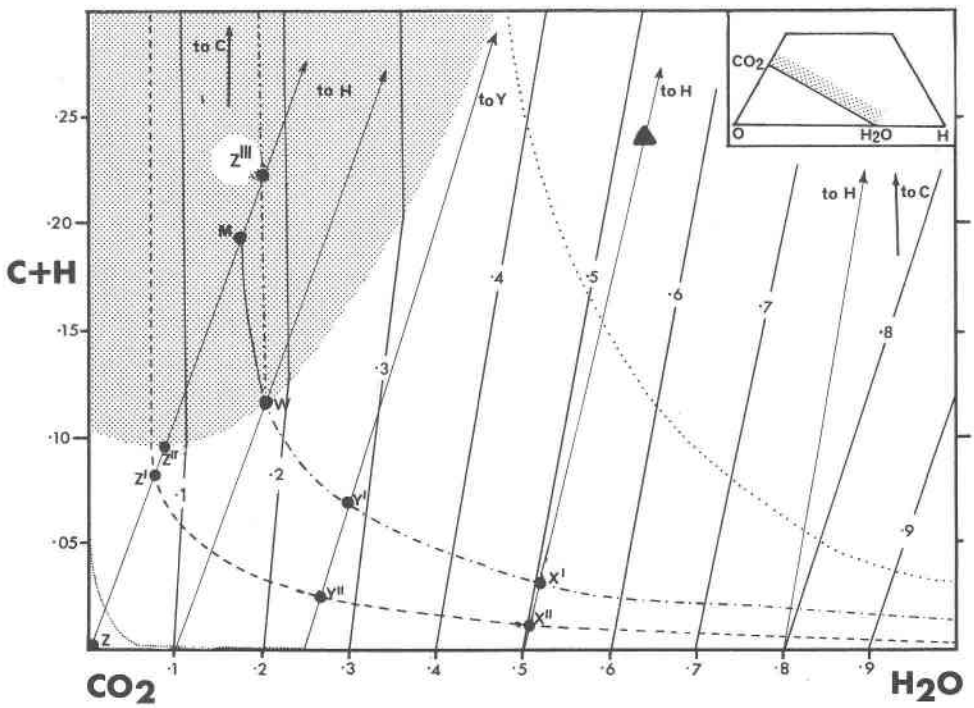

FIG. 3. Expanded scale diagram of a portion of the C–H–O system at 800°C and 1 kbar. The area pictured in the rectangular diagram is shown as the stippled area in the inset. Heavy solid lines are X_{H_2O} contours. Stippled area is in the graphite stability field. The symbols for hydrogen buffer contours are the same as for Figure 2 except that the dotted curve represents the $X_{H_2O} = 0.03$ contour. The solid triangle represents the initial composition of oxalic acid dihydrate. See text for further explanation.

the capsule, and the fluid composition will follow a hydrogen reaction line passing through X toward the H_2O–CO_2 join. The fluid reaches its equilibrium composition at X′ (the intersection of the hydrogen reaction line with the QFM, OH hydrogen buffer line). The value of X_{H_2O} in the fluid at X′ is 0.504, which can be estimated by interpolation between the 0.5 and 0.6 X_{H_2O} contours. X_{H_2O} in the equilibrium fluid is thus slightly greater than the nominal value of 0.500 calculated assuming loss of all H_2 in excess of $H_2O + CO_2$. If X_{H_2} in the system were controlled by NNO, OH, the equilibrium fluid composition would be given by X″ and the actual X_{H_2O} would be 0.502.

The same sort of behavior would be shown by a fluid generated by the decomposition of a mixture of oxalic acid dihydrate and anhydrous oxalic acid in 1:2 molar proportions. The initial fluid composition lies at Y in Figure 3, and changes along a hydrogen reaction line to reach equilibrium at Y′ or Y″ when the X_{H_2} is externally controlled by QFM, OH or NNO, OH respectively.

The decomposition of silver oxalate results in somewhat different behavior. The initial fluid composition corresponds to pure CO_2 (point Z in Figure 3) but if the external f_{H_2} corresponds to *e.g.*, NNO, OH, then H_2 diffuses into the capsule, reacts with CO_2 to produce H_2O and CO, and the fluid composition follows a hydrogen reaction line to Z′. X_{H_2O} in the supposedly pure CO_2 fluid is in fact = 0.06.

The Graphite Stability Field

Let us consider the decomposition of silver oxalate when X_{H_2} is controlled by QFM, OH. The initially pure CO_2 fluid would become progressively diluted with H_2 as the fluid composition follows the hydrogen reaction line from Z through Z′ to Z″, to intersect the graphite boundary. Graphite begins to precipitate at Z″, so that although the *bulk* composition continues to follow the hydrogen reaction line to Z‴, the *fluid* composition now follows a path from Z″ to W along the graphite boundary, while its C/O ratio changes due to the subtraction of C as graphite. Thus a fluid which was initially pure CO_2 reaches equilibrium at W with $X_{H_2O} = 0.17$! Graphite however, nucleates

very reluctantly, and it is quite possible that it might never precipitate during an experimental run. In these circumstances the fluid composition would continue to follow the hydrogen reaction line from Z″ towards Z‴ but would intersect the metastable QFM, OH hydrogen buffer line at the point **M**. The initially pure CO_2 fluid thus reaches metastable equilibrium at **M** with $X_{H_2O} = 0.15$.

Figures 4A–4F show that the graphite field expands with increasing P at constant T, and contracts with increasing T at constant P. The initial fluid composition resulting from the decomposition of oxalic acid dihydrate, plus the appropriate hydrogen reaction line, are shown in the Figure to demonstrate that the initial fluid composition of an excess H_2-generating compound may lie within the stability field of graphite during the initial stages of an experiment, when the system is under high pressure at low temperatures.

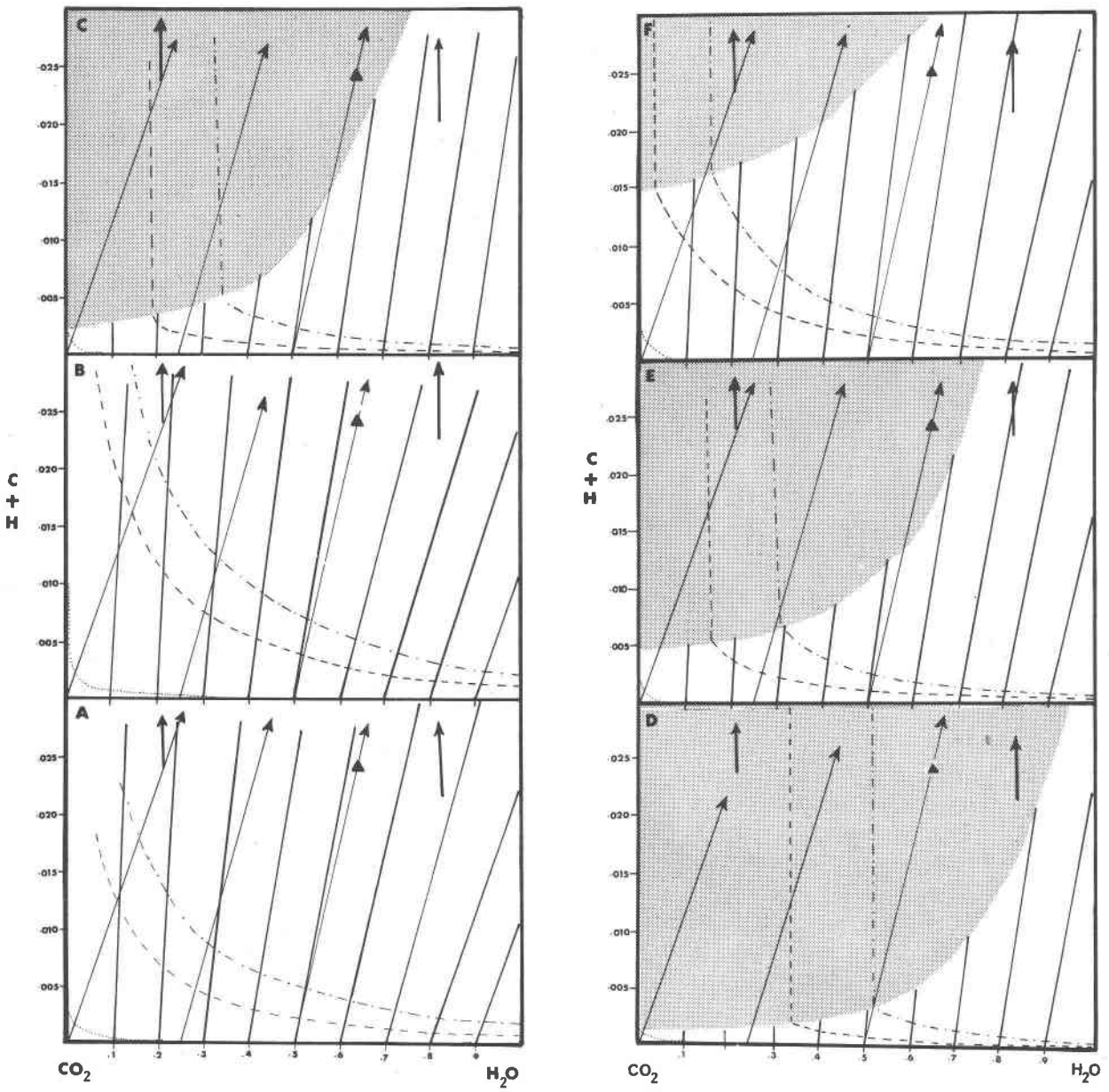

FIG. 4. Expanded scale diagrams similar to Figure 3. Symbols as in Figure 3. A. 1 kbar, 1000°C; B. 1 kbar, 1200°C; C. 5 kbar, 800°C; D. 10 kbar, 800°C; E. 10 kbar, 1000°C; F. 10 kbar, 1200°C.

There is the real danger that graphite may precipitate and persist metastably, as evidenced by the sporadic appearance of graphite in experimental run products.

X_{H_2O} and X_{H_2} contours for other P, T conditions are shown in Figure 4. Both the position of the hydrogen buffer lines and the slope of the X_{H_2O} contours change with P and T. Thus for a particular hydrogen buffer δ_{H_2O} ($= X(\text{real})_{H_2O} - X(\text{nom})_{H_2O}$) increases with P and decreases with increasing T, except in regions where the graphite boundary overlaps the hydrogen buffer line. The magnitude of δ_{H_2O} is small ($<\pm.015$) in the range $1.0 > X(\text{nom})_{H_2O} > 0.4$ and increases rapidly between $0.4 > X(\text{nom})_{H_2O} > 0.0$.

X_{CO_2} contours at 800°C, 1 kbar are shown in Figure 5. The overall position and slope of the contours remains much the same at other P, T conditions, but at any given P and hydrogen fugacity buffer the minor species CO becomes increasingly important as temperatures increase.

Variation of f_{O_2} with X_{H_2O}

In either the C–H–O or C–O–H–N systems at a given P and T, if X_{H_2} in the fluid has a fixed value, then f_{O_2} is dependent on X_{H_2O} in the fluid. This relationship is discussed by Whitney (1972) who shows that, if X_{H_2} remains constant, then decreasing X_{H_2O} from 1.0 to 0.25 lowers f_{O_2} by slightly more than one order of magnitude.

II. The System C–O–H–N

Introduction

The system C–H–O constitutes the base of the C–H–O–N tetrahedron shown in Figure 1B. Equilibrium calculations for the quaternary system show that N is almost invariably represented by the species N_2 under the usual range of experimental conditions. Consequently, fluid composition paths for which the ratio N/(C + H + O) is constant can be projected without distortion from the N apex onto the base of the tetrahedron.

The horizontal plane N/(C + H + O) = 2/3 (see Fig. 1B) was selected to illustrate various features of the quaternary system, and equilibrium calculations were carried out for compositions in this plane. The plane can be subdivided into four regions similar to those described for the C–H–O system (Figure 2), except that N_2 is now a major species throughout the plane. Assuming complete loss of excess H_2, a fluid generated by the decomposition of guanidine nitrate

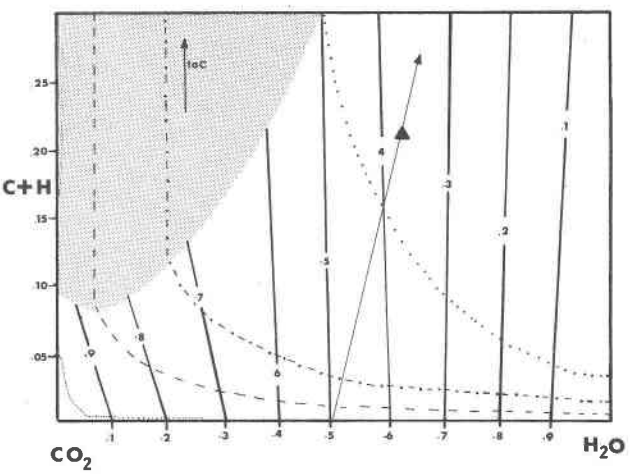

FIG. 5. Expanded scale diagram similar to Figure 3 showing X_{CO_2} contours as heavy solid lines. Other symbols as in Figure 3.

(Table 2) lies exactly in this plane, on its intersection with the vertical H_2O–CO_2–N plane (stippled in Figure 1B).

Figure 6A shows the N/(C + H + O) = 2/3 plane contoured for X_{H_2}. In Figure 6B the MH, NNO, and QFM (OH fluid) hydrogen buffers and graphite boundary (dashed lines) are projected from the N/(C + H + O) = 2/3 plane onto the base of the tetrahedron. The buffers and boundary curve for the quaternary system are displaced relative to those of the C–H–O system because the presence of N_2, essentially an inert dilutant, changes the mole fraction of the other fluid species.

The Effect of f_{H_2} on Fluid Compositions

A C–O–H–N fluid generated by the decomposition of a compound producing excess H_2 (Table 2) follows a path through the tetrahedron along a hydrogen reaction line. The variation in species composition along such a path is illustrated in Figure 7 in which, for a fluid produced by guanidine nitrate, the mole fractions of various species at constant P and T are plotted against X_{H_2}. Table 3 contains the results of the equilibrium calculations for this particular example. Appendix II (see footnote 1) contains the results of equilibrium calculations for oxalic acid dihydrate, guanidine nitrate, anhydrous oxalic acid (or silver oxalate), ammonium oxalate, and a 2:1 mixture of anhydrous oxalic acid with oxalic acid dihydrate.

The Graphite Stability Field

The stability field of graphite is of considerable importance in the generation of C–O–H–N fluids.

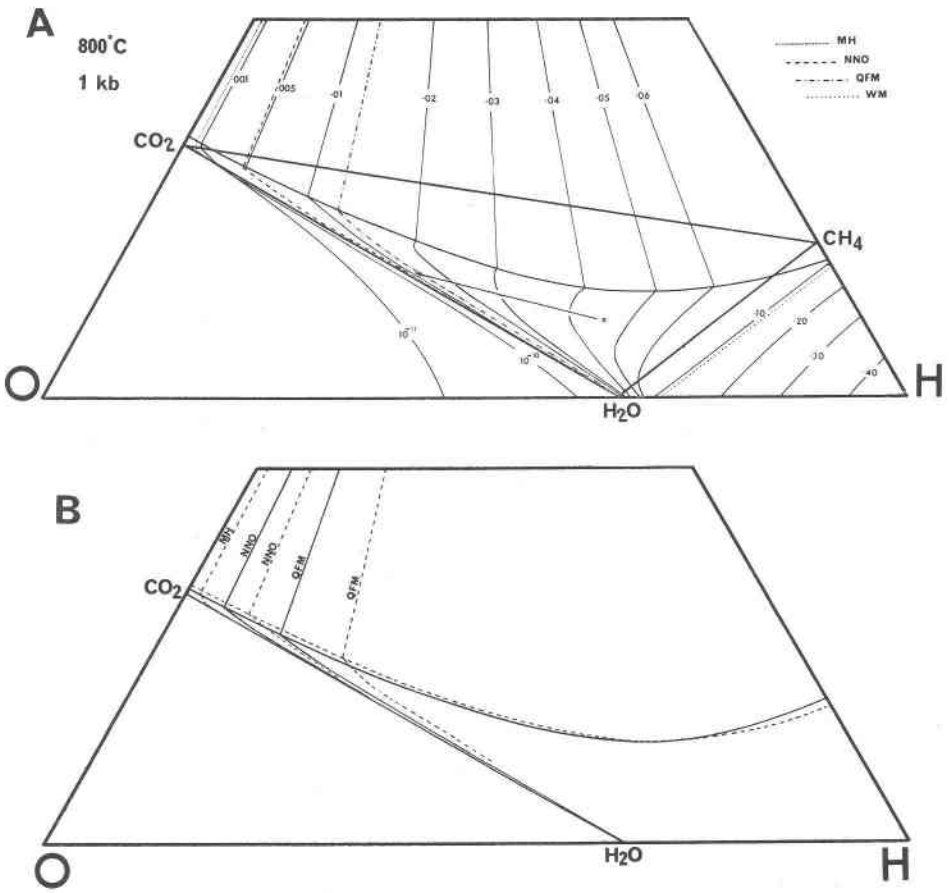

FIG. 6. A. A section through the C–O–H–N system projected onto the C–H–O base. The ratio of N/(C + O + H) = 3/2. Numbers on contours represent X_{H_2}. The fine dashed line represents the MH, OH hydrogen buffer contour, other symbols as in Figure 2. B. Comparison of hydrogen buffer contours and graphite boundary curves from Figure 2 and Figure 6A.

As in the system C–H–O, a fluid composition moving towards equilibrium along a hydrogen reaction line may intersect the graphite stability field, with consequences that have been discussed in an earlier section of this paper. There is likewise the problem of the early nucleation and metastable persistence of graphite during an experiment.

P and T affect the stability field of graphite in the quaternary system in a manner analogous to that described for the C–H–O system.

Experimental Limitations and Techniques

Low X_{H_2O} Fluids

The results of the equilibrium calculations show that in order to produce fluids with $X_{H_2O} < 0.25$ anp with $X_{H_2O} \simeq X(\text{nom})_{H_2O}$, the value of X_{H_2} must be considerably lower than that produced by NNO, OH. Also, to generate fluids consisting of pure CO_2 or N_2 in which X_{H_2O} is effectively zero the value of X_{H_2} must not be much greater than that produced by MnO–Mn_3O_4, OH. Such low X_{H_2} levels may be difficult to attain in some pressure vessels, especially solid-media apparatus with graphite furnaces and talc or pyrophyllite media. One possible remedy is to surround the sample capsule with an H_2 sink such as hematite (Millhollen, Wyllie, and Burnham, 1971). A second method which could be used in conjunction with the first would be to surround the sample with a phase which would decompose to CO_2. These large amounts of CO_2 would lower f_{H_2O} in the capsule surroundings, and in conjunction with hematite greatly lower f_{H_2} (*cf* Whitney, 1972).

Suppression of Graphite

The formation of graphite during the initial part of an experiment can be suppressed in some cases

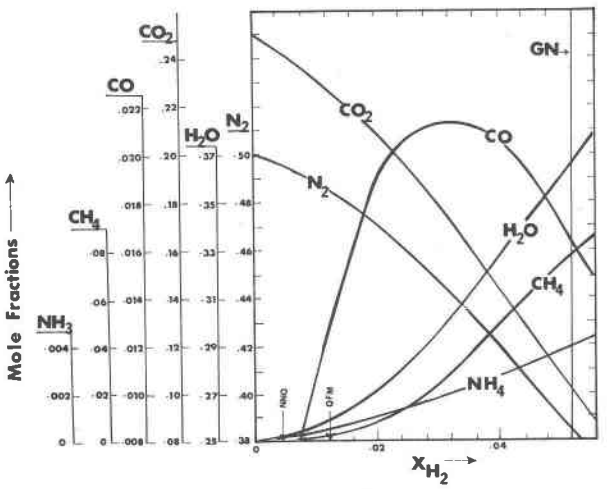

FIG. 7. Variation in the mole fraction of species in fluid produced by the decomposition of guanidine nitrate as a function of X_{H_2} at 800°C, 1 kbar. The vertical line labeled GN indicates the X_{H_2} value for the initial guanidine nitrate composition. The arrows labeled NNO and QFM indicate X_{H_2} value for NNO, OH and QFM, OH.

by using a combination of starting materials which together do not decompose to produce a large quantity of excess H_2. For example, a combination of PtO_2 + anhydrous oxalic acid could replace oxalic acid dihydrate, and the decomposition of the mixture would be as follows:

$$\tfrac{1}{2}PtO_2 + H_2C_2O_4 = 2CO_2 + H_2O$$

with no excess H_2 produced. In situations where a fluid which nominally consists of pure CO_2 is required, silver oxalate would be a better starting material than the excess H_2-producing anhydrous oxalic acid.

Changes in Fluid Composition by Reaction with Condensed Phases

The fluid phase composition may differ from that predicted if reaction with the condensed phases occurs. The fluid composition after reaction with the volatile species can be calculated, and the change is usually small or negligible when the fluid/condensed phase ratio is high. At high values of X_{H_2O}, a high ratio of fluid to condensed phase results in solution of large quantities of condensed phases in the fluid, but Holloway (1971) and Shettel (1973) have shown that a reduction of X_{H_2O} from 1.0 to 0.5 causes an exponential decrease in solute concentration. Holloway and Burnham (1972) found that a fluid/condensed phase ratio of 1:1 by weight was sufficient to maintain X_{H_2O} in the fluid within ±2 percent during hypersolidus runs in the system basalt-H_2O-CO_2.

Formation of Nitrides and Oxynitrides

The formation of nitrides and oxynitrides depends on the ratio P_{N_2}/P_{O_2}. Atmospheric pressure data indicate that the most stable simple metal nitrate FeN is stable at P_{N_2}/P_{O_2} ratios $> 10^{20}$ (Muan and Osborn, 1965). Few data exist for the more complex oxynitrides, but Ryall and Muan (1969) have shown that in the system Si–O–N, silicon oxynitride is stable at P_{N_2}/P_{O_2} ratios $> 10^{15}$. The effect of total pressure on the ratios should be small. These data suggest that, at low f_{O_2}, oxynitrides could form in silicate systems at high nitrogen pressures.

Acknowledgments

This work was supported by an Arizona State University Faculty Fellowship and grant GA-32442 from the National Science Foundation. Thanks are due to the staff of the Arizona State University Computation Center for aid in the machine computations. Bonnie J. McBride of the NASA Lewis Research Center kindly supplied us with a tape of the original equilibrium program. Reviews of an earlier version of the manuscript by G. B. Skippen and D. R. Waldbaum resulted in many improvements. Any clarity in our presentation is due to the comments of S. E. Kesson.

References

BURNHAM, C. W., J. R. HOLLOWAY, AND N. F. DAVIS (1969) Thermodynamic properties of water to 1,000°C and 10,000 bars. *Geol. Soc. Am. Spec. Pap.* **132,** 96 p.

DAYHOFF, M. O., E. R. LIPPINCOTT, R. V. ECK, AND G. NAGARIJAN (1967) Thermodynamic equilibrium in prebiological atmospheres of C, H, O, N, P, S, and Cl. *NASA Sp-***3040,** 259 pp.

EDMISTER, W. C. (1968) Applied hydrocarbon thermodynamics, Part 32, compressibility factors and fugacity coefficients from the Redlich-Kwong equation of state. *Hydrocarbon Process.* **47,** 239–244.

EUGSTER, H. P., AND G. B. SKIPPEN (1967) Igneous and metamorphic reactions involving gas equilibria. In, P. H. Abelson, Ed., *Researches in Geochemistry,* **2,** 492–520.

FRENCH, B. (1966) Some geological implications of equilibrium between graphite and a C–H–O gas at high temperatures, and pressures. *Rev. Geophys.* **4,** 223–253.

———, AND H. P. EUGSTER (1965) Experimental control of oxygen fugacities by graphite-gas equilibriums. *J. Geophys. Res.* **70,** 1529–1539.

GORDON, S., AND B. J. MCBRIDE (1971) Computer program for calculations of complex chemical equilibrium compositions, rocket performance, incident and reflected shocks, and Chapman-Jouquet detonations. *NASA SP-***273,** 245 p.

GREENWOOD, H. J. (1967) Mineral equilibria in the system MgO–SiO_2–H_2O–CO_2, In, P. H. Abelson, Ed. *Researches in Geochemistry,* **2,** 542–567.

HOLLOWAY, J. R. (1971) Composition of fluid phase solutes in a basalt–H_2O–CO_2 system. *Geol. Soc. Am. Bull.* **82,** 233.

——— (1973) The system pargasite–CO_2–H_2O: A model for melting of a hydrous mineral with a mixed volatile fluid. I. Experimental results to 8 kbar. *Geochim. Cosmochim Acta,* **37,** 651–666.

———, AND C. W. BURNHAM (1972) Melting relations of basalt with equilibrium water pressure less than total pressure. *J. Petrol.* **13,** 1–29.

———, ———, AND G. L. MILLHOLLEN (1968) Generation of H_2O–CO_2 mixtures for use in hydrothermal experimentation. *J. Geophys. Res.* **73,** 6598–6600.

———, D. H. EGGLER, AND N. F. DAVIS (1971) An analytical expression for calculating the fugacity and free energy of H_2O to 10,000 bars and 1300°C. *Geol. Soc. Am. Bull.* **82,** 2639–2642.

HUEBENER, J. S. (1971) Buffering techniques for hydrostatic systems at elevated pressures. p. 123–177 in *Research Techniques for High Pressure and Temperature,* G. C. Ulmer, Ed., Springer-Verlag, New York.

HUFF, V. N., S. GORDON, AND V. E. MORRELL (1951) General method and thermodynamic tables for computation of equilibrium composition and temperature of chemical reactions. *Natl. Adv. Comm. Aeronaut.* (NACA) *Rep.* **1037.**

KENNEDY, G. C. (1954) Pressure-volume-temperature relations in CO_2 at elevated temperatures and pressures. *Am. J. Sci.* **252,** 225–241.

KESSON, S. E., AND J. R. HOLLOWAY (1974) The generation of N_2–CO_2–H_2O fluids for use in hydrothermal experimentation. II. Melting of albite in a multispecies fluid. *Am. Mineral.,* **59,** 598–603.

LEWIS, G. N., AND M. RANDALL (1961) *Thermodynamics,* revised by K. S. Pitzer and L. Brewer, 2nd ed., McGraw-Hill Book Co., New York, 723 p.

MATTHEWS, J. F. (1972) The critical constants of inorganic substances. *Chem. Rev.* **72,** 71–100.

METZ, P. (1967) Experimentelle Bildung von Forsterit und Cacitaus Tremolite und Dolomite. *Geochim. Cosmochim. Acta,* **31,** 1517–1532.

MILLHOLLEN, G. L., P. J. WYLLIE, AND C. W. BURNHAM (1971) Melting relations of $NaAlSi_3O_8$ to 30 Kb in the presence of H_2O:CO_2 = 50:50 vapor. *Am. J. Sci.* **271,** 473–480.

MUAN, A., AND E. F. OSBORN (1965) *Phase Equilibria Among Oxides in Steelmaking.* Addison-Wesley Pub. Co., Inc. Reading, Mass., 236 p.

PRESNALL, D. C. (1969) Pressure-volume-temperature measurements on hydrogen from 200° to 600°C and up to 1800 atmospheres. *J. Geophys. Res.* **74,** 6026–6033.

REDLICH, O., AND J. N. S. KWONG (1949) On the thermodynamics of solutions: V. An equation of state. Fugacities of gaseous solutions. *Chem. Phys.* **44,** 233.

REESE, R. L. (1973) *Computed Solid-Vapor Equilibria in Multicomponent Systems.* M.S. Thesis, Arizona State University, Tempe, Arizona.

ROBIE, R. A., AND D. R. WALDBAUM (1968) Thermodynamic properties of minerals and related substances at 298.15°K (250°C) and one atmosphere (1.013 bars) pressure and at higher temperatures. *U.S. Geol. Surv. Bull.* **1259,** 256 p.

RYALL, W. R., AND A. MUAN (1969) Silicon oxynitride stability. *Science,* **165,** 1363–1364.

SHARP, W. E. (1962) The thermodynamic functions for carbon dioxide in the range 40–1000°C and 1 to 1400 bars. *UCRL-7168, Chem. UC-4, TID* **4500,** 52 p.

SHAW, H. R. (1963) Hydrogen-water vapor mixtures: control of hydrothermal atmospheres by hydrogen osmosis. *Science,* **139,** 1220–1222.

——— (1967) Hydrogen osmosis in hydrothermal experiments. In, P. H. Abelson, Ed. *Researches in Geochemistry,* **2,** John Wiley and Sons, New York, 521 p.

———, AND D. R. WONES (1964) Fugacity coefficients for hydrogen gas between 0° and 1000°C for pressures to 3000 atm. *Am. J. Sci.* **262,** 918–929.

SHETTEL, D. L. (1973) Solubility of quartz in H_2O–CO_2 fluids at 5 Kb and 500–900°C. *Trans. Am. Geophys. Union,* **54,** 480.

STULL, D. R., AND H. PROPHET (1971) *JANAF Thermochemical Tables.* Second ed., *Nat. Bur. Stand.* NSRDS-NBS **37.**

VAN ZEGGERN, F., AND S. H. STOREY (1970) *The Computation of Chemical Equilibrium.* Cambridge University Press, 176 p.

WHITNEY, J. A. (1972) The effect of reduced water fugacity on the buffering of oxygen fugacity in hydrothermal experiments. *Am. Mineral.* **57,** 1902–1908.

Manuscript received, October 27, 1972; accepted for publication, October 12, 1973.